Proceedings of DETC 2001
2001 ASME Design Engineering Technical Conferences
September 09-12, 2001, Pittsburgh, Pennsylvania, USA

STOCHASTIC NONLINEAR DYNAMICS OF A BEAM SYSTEM WITH IMPACT

N. van de Wouw, A. de Kraker, H. Nijmeijer
Eindhoven University of Technology,
Department of Mechanical Engineering,
P.O. Box 513, 5600 MB Eindhoven,
The Netherlands
N.v.d.Wouw@tue.nl

Abstract

In this paper, a strongly nonlinear beam-impact system under both broad-banded and small-banded, Gaussian noise excitations is investigated. The response of this system is investigated both numerically, through a multi-degree-of-freedom (MDOF) model, and experimentally focusing on frequency-domain characteristics such as stochastic equivalents of harmonic and subharmonic solutions. Improved understanding of these stochastic response characteristics is obtained by comparing them to nonlinear periodic response features of the system. It will be shown that in modeling such a continuous linear system with a local nonlinearity, the linear part can be effectively reduced to a description based on several modes. Combining this reduced linear part with the local nonlinearity in a reduced nonlinear model is shown to result in an analysis model, which can be used to accurately predict the stochastic response characteristics of the original, continuous, nonlinear system. It is shown that the inclusion of more modes in the model will result in a response, which differs significantly from that of a SDOF (single-degree-of-freedom) model, giving a better correspondence with experimental results, also in the frequency range of the first mode.

1 Introduction

Nonlinear, dynamic systems forced by random excitations are often encountered in practice. The source of randomness can vary from surface randomness in vehicle motion, environmental changes, such as earthquakes and wind exciting high rise buildings or wave motions at sea exciting offshore structures or ships, to electric or acoustic noise exciting mechanical structures. Often these stochastic excitations exhibit a colored frequency spectrum. Moreover, many practical, nonlinear systems comprise a continuous linear part and a local nonlinearity.

In this paper, a system, representative for the class of systems mentioned above, namely, a base-excited beam system with a nonlinear elastic stop is investigated. Systems with elastic stops are typical examples of systems with local nonlinearities and represent a wide range of practical nonlinear dynamic systems. Examples are gear rattle, ships colliding against fenders, suspension bridges and snubbers in solar panels on satellites. Although the nonlinearity is local, the dynamic behavior of the entire system is influenced by it. Nonlinear periodic response phenomena of these kind of systems have been studied extensively [1; 2; 3; 4]. Moreover, a study of the stochastic response characteristics of a SDOF model of this system can be found in [5].

When stochastic excitations are applied to the nonlinear beam system, it features many interesting, stochastic, nonlinear response phenomena. These phenomena are of specific interest because they shed light on the common characteristics of periodic and stochastic dynamic behavior. As a consequence, the behavior of the system can be understood more thoroughly. The stochastic nonlinear response phenomena will be studied numerically as well as experimentally. For the numerical investigations a model is used, in which the linear, continuous part of the system (the elastic beam) is reduced to a multiple-mode description. It will be shown that the model obtained by the reduction of the linear, continuous part of the system (the elastic beam) based on a limited number of elastic modes can accurately describe the stochastic response of the experimental system. The comparison of numerical and experimental results will display the added value of the MDOF model when compared with a SDOF model [5]. Herein, the applied, stochastic excitations are

Gaussian and have a band-limited power spectral density. Still, these excitations can be realizations of broad-banded or narrow-banded processes. It should be noted that particularly the nonlinear phenomena in the power spectral density of the response will be investigated extensively.

In the next section, we introduce the nonlinear dynamic system and its 2DOF model. In section 3, a brief survey of simulated periodic response characteristics will be given. In section 4, the simulation approach for stochastic excitations will be treated and the related simulation results will be discussed in section 5. In section 6, we present the experimental set-up. Furthermore, in section 7, the simulation results are compared to the experimental results. Finally, in section 8, we present some conclusions.

2 The nonlinear beam system

2.1 System description

The nonlinear, dynamic system comprises a linear elastic beam, which is clamped onto a rigid frame, and an elastic stop, see figure 1. The elastic stop consists of two ptfe (teflon) half spheres. The system is excited by a prescribed, stochastic *displacement* $y(t)$ (with respect to a fixed reference position of the frame) of the rigid frame. The response $x(z,t)$ is the vertical *displacement* (with respect to a fixed reference position of the frame) of the beam at the horizontal coordinate z. Firstly, in section 2.2, the approach in building a MDOF model for the elastic beam will be illuminated. Next, in section 2.3, a model for the elastic stop will be presented. The estimation of the parameters, describing the nonlinearity, is based on experiments and will be elucidated in that section. Finally, in section 2.4, a nonlinear, two-degree-of-freedom (2DOF) model of the beam-impact system will be discussed.

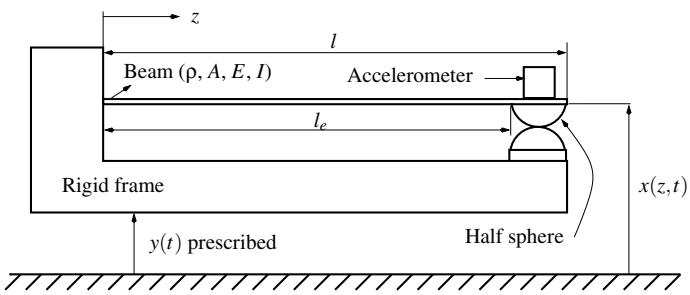

Figure 1. The nonlinear, base-excited beam system with Young's modulus $E = 1.9\ 10^{11}$ N/mm^2, density $\rho = 8000$ kg/m^3 , cross-section $A = 58.3$ mm^2, second moment of area of the cross-section $I = 18.5$ mm^4, length $l = 259.9$ mm ($l_e = 229$ mm), mass of a half sphere $m_s = 12.4\ 10^{-3}$ kg and mass of the accelerometer $m_a = 13.0\ 10^{-3}$ kg.

2.2 Modeling the elastic beam

For the elastic beam shear effects and rotational inertia will be neglected (Euler beam). In a first step, spatially discretized models for such a continuous system can be derived using the Rayleigh-Ritz method [6]. This method was applied to obtain a 4DOF model of the elastic beam, where the half sphere and the accelerometer have been modeled as rigid parts at $z = \frac{l+l_e}{2}$. Additional evaluations showed that a reduction of the 4DOF model to a model incorporating only the two modes corresponding the lowest two eigenfrequencies is very acceptable with respect to our research goal. Moreover, these eigenfrequencies match their experimental equivalents quite well, see table 1. Therefore, the 4DOF model was reduced to a 2DOF model using only these first two eigenmodes of the 4DOF model [7]. In figure 2, the modes corresponding to these eigenfrequencies are displayed. Moreover, corresponding dimensionless damping parameters are given, which were estimated by experimental means.

Eigenfrequencies [rad/s]	
Experimental	Model
101.5	109.1
781.6	790.7

Table 1. Lowest two eigenfrequencies of the 4DOF model vs. experimental eigenfrequencies.

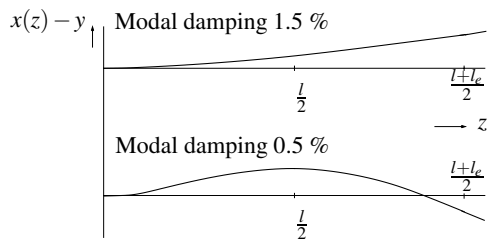

Figure 2. Modes shapes and modal damping parameters corresponding to the lowest two eigenfrequencies.

2.3 Modeling the elastic stop

The elastic stop is modeled using a Hertzian contact model [8; 9]. Using the Hertzian model, the following relationship holds between the contact force F and the relative displacement

of the two colliding spheres $\delta = y - x(z = \frac{l+l_e}{2})$:

$$F = \frac{2}{3} E_r \sqrt{R_r}\, \delta^{1.5} = K_{\text{Hertz}}\, \delta^{1.5} \qquad \text{for} \quad \delta \geq 0. \tag{1}$$

In (1), the reduced Young's modulus E_r reflects the material properties of both colliding bodies. Furthermore, the reduced radius of curvature R_r reflects the geometric properties of the colliding bodies. These parameters are defined by $E_r = \frac{E}{1-\nu^2}$, $R_r = R/2$, where E, ν, and R are the Young's modulus, the Poisson's ratio, and the principal radius of curvature of the half spheres (identical half spheres assumed).

The contact model (1) can be refined by adding a hysteretic damping term, see [10], accounting for energy loss during collision. The inclusion of hysteretic damping alters (1) to:

$$\begin{aligned} F &= K_{\text{Hertz}}\, \delta^{1.5} \left(1 + \frac{\mu}{K_{\text{Hertz}}} \dot{\delta}\right) \\ &= K_{\text{Hertz}}\, \delta^{1.5} \left[1 + \frac{3(1-e^2)}{4} \frac{\dot{\delta}}{\dot{\delta}^-}\right] \quad \text{for } \delta \geq 0, \end{aligned} \tag{2}$$

in which e is the coefficient of restitution, a geometry and material dependent measure for energy dissipation. Moreover, $\dot{\delta}^-$ represents the velocity difference of the two colliding bodies at the beginning of the collision.

The parameters K_{Hertz} and e were determined experimentally ($K_{\text{Hertz}} = 2.1\ 10^8$ N/m$^{1.5}$, $e = 0.5$). Both K_{Hertz} and e are obtained as least-squares estimates in which the information from several collisions is accounted for. The underlying experiment resulted in information regarding the indentation δ, the indentation velocity $\dot{\delta}$, and the contact force F. The dependency of the contact force F between the colliding half spheres on the indentation δ is visualized in figure 3. The parameter K_{Hertz} can be estimated by comparing the contact force F and the indentation δ at maximum indentation ($\dot{\delta} = 0$), assuming that the static contact force is proportional to $\delta^{1.5}$, see equation (1). The coefficient of restitution e can be estimated by considering the amount of energy loss ΔT during a collision. ΔT is equal to the surface within the hysteresis loop: $\Delta T = \oint \mu\, \delta^{1.5}\, \dot{\delta}\, d\delta$. Therefore, μ can be estimated from $\mu = \frac{\Delta T}{\oint \delta^{1.5}\, \dot{\delta}\, d\delta}$. The coefficient of restitution can now be obtained from:

$$e = \sqrt{1 - \frac{\frac{4}{3}\, \mu \dot{\delta}^-}{K_{\text{Hertz}}}}. \tag{3}$$

2.4 The nonlinear dynamical model

In the previous two sections, the two components of the beam-impact system, namely, the beam and the elastic stop, were discussed. The assembled, nonlinear model can be described by the following set of equations of motion:

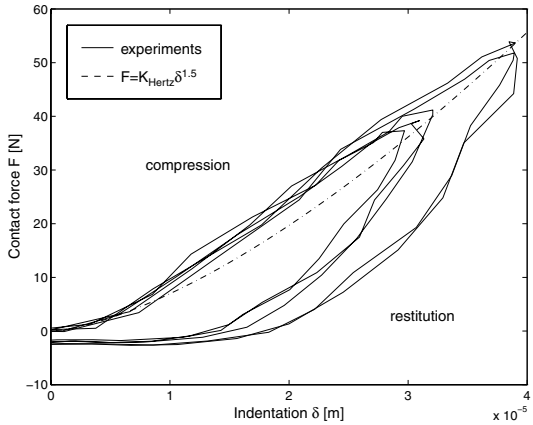

Figure 3. Measurement of several collisions to estimate K_{Hertz} and e.

$$\begin{aligned} &\underline{M}\,\ddot{\underline{n}} + \underline{C}\,\dot{\underline{n}} + \underline{K}\,\underline{n} + \underline{K}_{\text{H}}\, \varepsilon(\delta)\, \delta^{1.5} \left(1 + \frac{3(1-e^2)\,\dot{\delta}}{4\,\dot{\delta}^-}\right) = \underline{m}_0 \ddot{y}, \\ &\text{with} \quad \varepsilon(\delta) = \begin{cases} 1 \text{ for } \delta > 0 \\ 0 \text{ for } \delta \leq 0 \end{cases}. \end{aligned} \tag{4}$$

Herein, $\underline{n}$ is a column matrix (of length two) of natural coordinates, which represent the contribution of the two modes to the total response, whereas $\underline{M}$ and $\underline{K}$ are the mass matrix and stiffness matrix, respectively, following from the Rayleigh-Ritz procedure. $\underline{C}$ represents the damping matrix which takes into account the measured modal damping (see figure 2). Moreover, $\underline{K}_{\text{H}}$ is a coefficient matrix of the nonlinearity while the term, in which $\underline{m}_0$ is involved, expresses the fact that the excitation is a prescribed displacement. Additionally, δ is the first component of $\underline{\delta} = [\delta,\ \delta_m]^T := \left[y - x(z = \frac{l+l_e}{2}),\ y - x(z = \frac{l}{2})\right]^T$, representing the relative displacement of the beam with respect to the rigid frame at the point of contact of the two half spheres. Note that $\underline{\delta}$ can be written as a linear combination of the components of $\underline{n}$. Moreover, in (4) $\dot{\delta}$ represents the relative velocity at the same point.

This model will now be used to simulate (through numerical time integration) the nonlinear response $\underline{\delta}$ for different excitation forms $y = y(t)$.

3 Survey of simulated response to periodic excitation

In order to enlarge the ability to interpret the stochastic response phenomena, to be discussed later on in this paper, we present some periodic response phenomena of the nonlin-

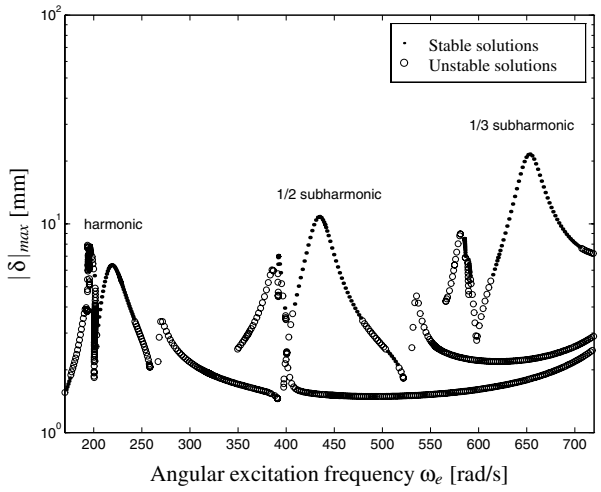

Figure 4. Maximum, absolute displacements $|\delta|_{max}$ of periodic solutions of the 2DOF beam-impact system.

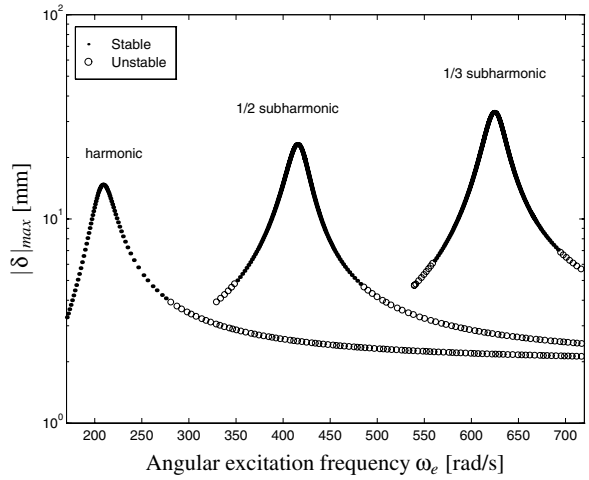

Figure 5. Maximum, absolute displacements $|\delta|_{max}$ of periodic solutions of the SDOF beam-impact system.

ear beam system. In figure 4, the maximum, absolute displacements $|\delta|_{max}$ (of the periodic solutions) are plotted against the angular frequency ω_e of the periodic (harmonic) base-excitation $y = y(t)$. These data were obtained using a periodic solver and a path-following procedure [1; 3]. Some important nonlinear response characteristics can be extracted from figure 4. Firstly, besides the harmonic resonance, corresponding to the first linear eigenmode of the elastic beam, related subharmonic resonances appear. Secondly, a remarkable feature can be found in the fact that the maximum absolute values of the subharmonic solutions are higher than those of the harmonic solutions. Finally, a striking characteristic is expressed by the fact that both the harmonic and subharmonic resonance peaks exhibit large dents near their resonance frequencies. In figure 5, it is shown that this effect is absent in the periodic response of a SDOF model [7] of the beam-impact system that it is, therefore, most likely caused by the presence of the second mode in the model. Note in this respect that the second harmonic resonance frequency (780 rad/s) lies at four times the frequency at which the first harmonic resonance shows a dent (195 rad/s). This typically nonlinear characteristic was also observed in experiments [11]. Clearly, the inclusion of extra 'modes' in the model not only affects the response in the neighborhood of the resonance frequency of this 'mode', but also influences the response characteristics at lower frequencies dramatically.

4 Simulation approach for Gaussian excitation

4.1 Generation excitation signals

As mentioned before, the excitation form applied to the nonlinear beam system is Gaussian, band-limited noise. Now, we would like to be able to generate realizations of such a Gaussian excitation process, which exhibits the desired power spectral density $S_{yy}(\omega)$. The energy of a band-limited, random process is concentrated in the frequency band $\omega_{band} = [\omega_{min},\ \omega_{max}]$ (for both positive and negative frequencies). For any shape of the power spectral density of the Gaussian process, within that frequency band, one can simulate realizations of such a process using a method developed in [12] and [13]. The idea behind the method is that a one-dimensional Gaussian, random process $y(t)$ with zero mean and a one-sided power spectral density $S^o_{yy}(\omega)$, with

$$S^o_{yy}(\omega) = \begin{cases} 2\,S_{yy}(\omega) & \text{for } \omega > 0 \\ S_{yy}(\omega) & \text{for } \omega = 0 \\ 0 & \text{for } \omega < 0 \end{cases}, \tag{5}$$

can be approximated by a finite sum of cosine functions with a uniformly distributed random phase Φ. A realization $\bar{y}(t)$ of $y(t)$ can be simulated by $\bar{y}(t) = \sqrt{\Delta\omega}\,\mathrm{Re}\{F(t)\}$, in which $\mathrm{Re}\{F(t)\}$ is the real part of $F(t)$ and

$$F(t) = \sum_{k=1}^{N} \left\{ \sqrt{2\,S^0_{yy}(\omega_k)}\; e^{i\phi_k} \right\} e^{i\omega_k t} \tag{6}$$

is the finite complex Fourier transform of $\sqrt{2\,S^o_{yy}(\omega)}\; e^{i\phi}$, in which ϕ is a realization for Φ, and $\Delta\omega = \omega_k - \omega_{k-1}$.

Next, we can obtain a realization of the response process using classical numerical integration techniques.

4.2 Numerical time integration

Numerical time integration is used to compute time series of the response $\delta(t)$. The computed realizations of the response can be used to estimate the invariant measures of the stationary solutions, such as statistical moments, probability density function and power spectral density.

The accuracy of the estimates of the stochastic invariants depends on the length of the time series used (corresponding to a statistical error on the estimate of the stochastic invariant) and the integration accuracy underlying the time series. Therefore, the efficiency of the integration technique is an important issue. Variable step size schemes, in which stability checks and accuracy checks are performed at each integration step, are rather inefficient for our purpose. Therefore, a constant step-size Runge-Kutta scheme is used. Since explicit integration schemes are only conditionally stable, a minimum step size (that ensures stability) can be determined. Due to the major difference in stiffness between contact and non-contact situations, the minimal step sizes for these situations differ enormously. It would be very inefficient to choose one single constant step size based on contact situations. Therefore, two different stable step sizes are used. Consequently, the time of impact has to be determined accurately (and in a computationally efficient manner) to avoid entering contact with the large integration time step. For this purpose the Hénon method [7; 14] is implemented within the integration routine.

5 Simulation results for Gaussian excitation

Here, the simulation results will be discussed. The excitations $y(t)$, applied to the model, are realizations of Gaussian, band-limited stochastic processes. The target spectrum[1] of the excitation is taken uniformly distributed within a limited frequency band $\omega_{band} = [\omega_{min}\ \omega_{max}]$ and its level is chosen to represent a physically sensible prescribed displacement of the rigid frame (order of maginitude 1 mm). First, a band excitation with $\omega_{band} = [0.0\ 1226.6]$ rad/s is applied to the system. This excitation is broad-banded relatively to the response characteristics depicted in figure 4. It should be noted that the excitation is Gaussian by nature of its generation.

In figure 6, the power spectral densities of the response variables δ and δ_m are shown. The contribution of the first eigenmode is clearly present near $\omega = 195$ rad/s. The contribution of the second mode of the linear beam to δ is now apparent around $\omega = 780$ rad/s. Note that the first nonlinear resonance frequency is almost twice the lowest linear eigenfrequency of the beam. In [15] it is stated that in a piece-wise linear system the nonlinear resonance frequency approaches twice the linear eigenfrequency (of the system without nonlinearity) for a very high nonlinearity. Since the impact phenomenon plays a less important role in the nonlinear response related to the second mode, the second resonance frequency is much lower than twice the second linear eigenfrequency of the beam. The contribution of the second degree of freedom becomes more evident when one observes the power spectral density of the response variable δ_m for the same excitation, see figure 6. The contribution of the second mode to the response of the system appears in a more dominant way in the mid-beam displacement (see figure 6), since the second mode has its maximum displacement near the middle of the beam, see figure 2. Note that, besides the resonances near 195 rad/s and 780 rad/s, extra resonance peaks occur, which represent higher harmonics of the resonance near 195 rad/s (related to the first linear eigenmode of the elastic beam). Furthermore, the response signal contains a large amount of energy at low frequencies ($\omega < 50$ *rad/s*). It is well-known that when the excitation, and therefore the response, contains two frequencies ω_1 and ω_2, the response can also contain the 'difference'-frequency $\omega_2 - \omega_1$ when the system exhibits an asymmetric stiffness nonlinearity. Note that broad-banded excitation contains a large number of nearby frequencies. Hence, a lot of interaction can be expected in this case. When those excitation frequencies lie in a resonance peak of the system, these 'difference'-frequencies will contain a significant amount of energy. Both phenomena were also observed in the response of the SDOF model of the beam-impact system [5] and other nonlinear systems with asymmetric stiffness nonlinearities [7].

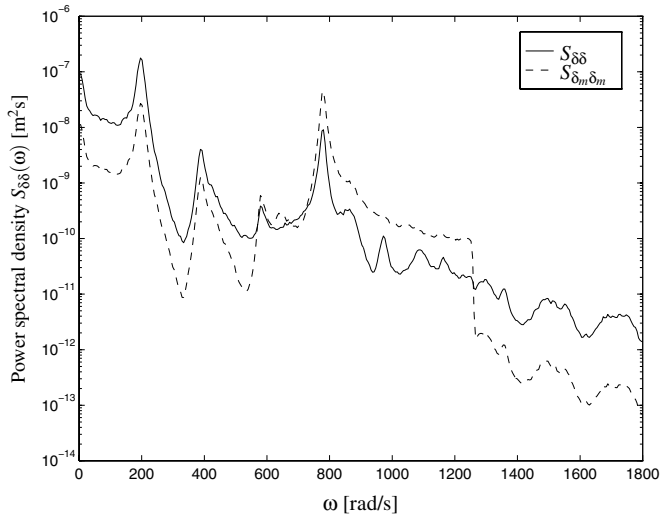

Figure 6. Power spectral densities of δ and δ_m for ω_{band} =[0.0 1226.6] rad/s.

In figure 7 , estimates for the probability density functions of the relative end-displacement δ and the relative mid-beam displacement δ_m are shown. Clearly, δ_m tends towards a Gaussian distribution. From a physical point of view, it is clear that δ_m

[1] It should be noted that for the remainder of this paper one-sided power spectral densities will be considered

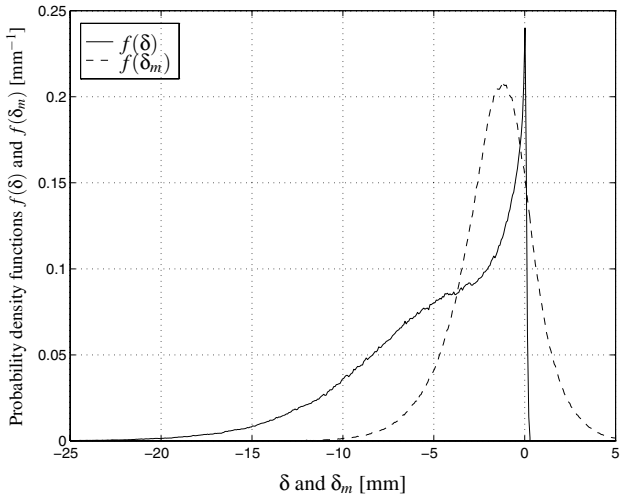

Figure 7. Probability density functions of δ and δ_m for ω_{band} =[0.0 1226.6] rad/s.

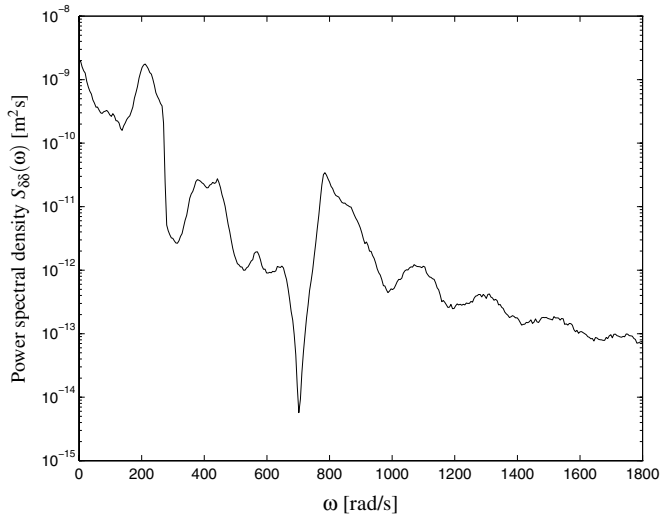

Figure 8. Power spectral density of δ for ω_{band} =[144.5 270.2] rad/s.

should not exhibit such an extreme asymmetry as δ, since the beam does not encounter a contact at the horizontal position $z = l/2$. From a more general point of view, it is known [16], that the output of a linear system, in case of a non-Gaussian input, will be closer to Gaussian than the input. In this perspective, we can view upon δ_m as an output of a linear system (the beam) with a non-Gaussian input δ. This tendency towards a Gaussian distribution becomes stronger for weakly damped systems.

Next, three different narrow-band excitations were applied:

1. a band-limited excitation, with $\omega_{band} = [144.5\ 270.2]$ rad/s, that covers the major part of the harmonic resonance peak, see figure 4;
2. a band-limited excitation, between $\omega_{band} = [351.9\ 477.5]$ rad/s, that covers the major part of the 1/2 subharmonic resonance peak, see figure 4.
3. a band-limited excitation, between $\omega_{band} = [559.2\ 684.9]$ rad/s, that covers the major part of the 1/3 subharmonic resonance peak, see figure 4.

It should be noted that all three excitation signals are realizations of Gaussian stochastic processes, which exhibit the same variance and have uniformly distributed energy within their specified frequency bands.

The power spectral densities of the responses to these excitations are displayed in the figures 8, 9 and 10. Note that a 'harmonic' solution of the nonlinear, 2DOF model to a harmonic excitation with frequency ω_e exists, see figure 4, and has a specific period time $\frac{2\pi}{\omega_e}$ but comprises multiple frequencies $\omega_e, 2\,\omega_e, 3\,\omega_e, \ldots$. Clearly, this is also the case for stochastic excitations, see figure 8. Moreover, remarkable, stochastic, nonlinear response phenomena are displayed in the figures 9

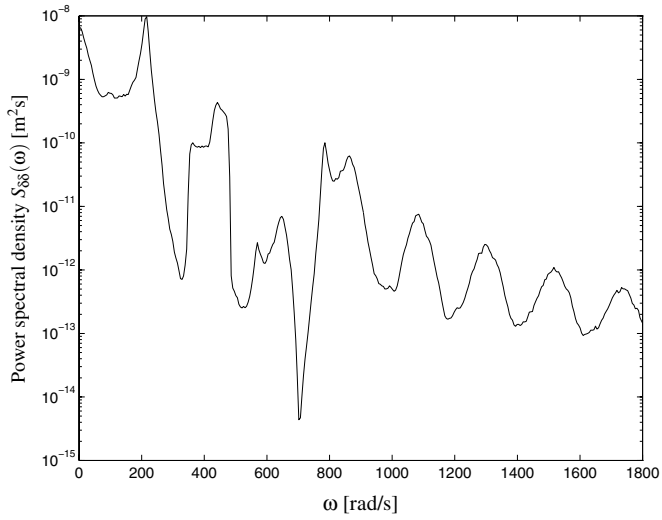

Figure 9. Power spectral density of δ for ω_{band} =[351.9 477.5] rad/s.

and 10. Namely, figure 9 shows a 'stochastic 1/2 subharmonic' solution and figure 10 shows a 'stochastic 1/3 subharmonic' solution. Note that in the same frequency range subharmonic solutions exist when the system is excited periodically, see figure 4. To be more specific, a 1/n subharmonic effect is responsible for the fact that the excitation frequency band $[\omega_{min}\ \omega_{max}]$ also results in an important response in the frequency range $[\frac{\omega_{min}}{n}\ \frac{\omega_{max}}{n}]$, see figure 9 and 10.

We can distinguish another, interesting, common characteristic of the periodic and stochastic response of the beam-impact system by comparing the figures 8, 9 and 10. Namely, the 'stochastic 1/3 subharmonic' solution contains significantly more

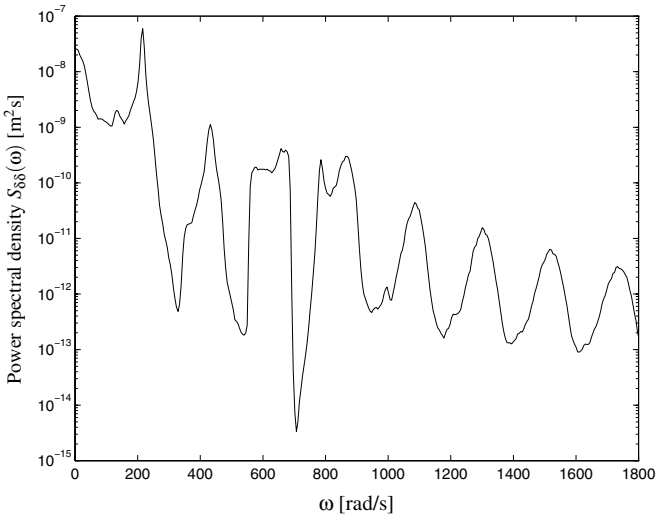

Figure 10. Power spectral density of δ for ω_{band} =[559.2 684.9] rad/s.

energy than the 'stochastic 1/2 subharmonic' solution, whereas the 'stochastic 1/2 subharmonic' solution contains significantly more energy than the 'stochastic harmonic' solution. Note that a comparable phenomenon was observed in the periodic response of the MDOF model of the beam-impact system, see figure 4.

6 Experimental set-up

In the next section, simulation results will be validated by comparison to experimental results. The experimental set-up is presented schematically in figure 11. A uniformly distributed, Gaussian, band-limited excitation signal is generated numerically using Shinozuka's method [12]. This signal is sent to a controller, which controls a servovalve using feedback information from an internal displacement transducer. The servovalve provides the input for the hydraulic actuator by controlling the oil flow of the hydraulic power supply. A hydraulic service manifold connects the hydraulic power supply and the servo-

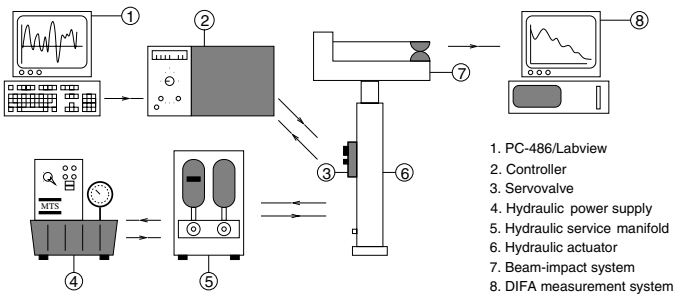

Figure 11. The experimental set-up of the beam-impact system.

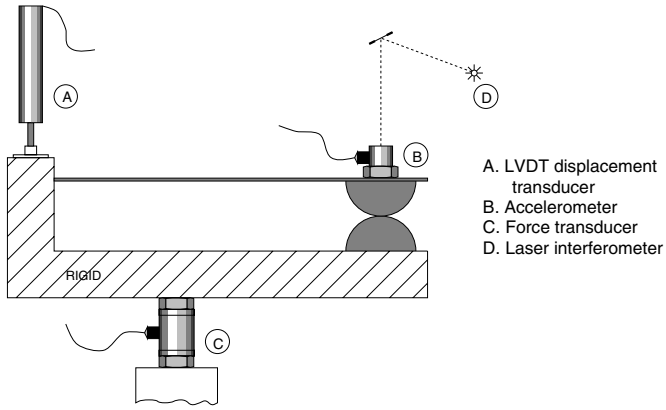

Figure 12. The measurement equipment.

valve. This service manifold reduces fluctuations and snapping in the hydraulic lines during dynamic programs. All measurements are monitored using the data acquisition software package DIFA [17].

Figure 12 shows the measurement equipment mounted on the beam-impact system. A Linear Variable Differential Transformer (LVDT) measures the displacement of the rigid frame. The displacement and velocity of the beam, at the point of contact, are measured by a laser interferometer. Furthermore, the acceleration of the beam is measured by an accelerometer and a force transducer is used to measure the force acting on the rigid frame, where the force transducer is positioned at the center of mass of the rigid frame and rotations of the rigid frame are assumed to be small. The rigid frame displacement measurements are used as input for the simulations described in the next section.

7 Experimental results

In section 5, several interesting, stochastic, nonlinear response characteristics were observed in the simulation results. Comparable phenomena are encountered in the experiments as well and will be discussed here. Moreover, the validity of the 2DOF model will be assessed by comparing the experimental results with the simulation results. Herewith, also the added value of the 2DOF model with regard to the SDOF model, as presented in [5], can be assessed.

A [0.0 1226.6] rad/s band excitation was applied. The realized excitation spectrum is depicted in figure 13. In contrast with the signal offered to the controller, the power spectral density of the actual rigid frame displacement is clearly not uniformly distributed within the specified frequency range. This is due to the fact that the hydraulic actuator behaves like a first-order low-pass filter. Both the simulated and measured power spectral densities of the response $\delta(t)$ are shown in figure 14. The most important response phenomena like higher harmonics, related to the resonance near 195 rad/s, and the presence of a large amount

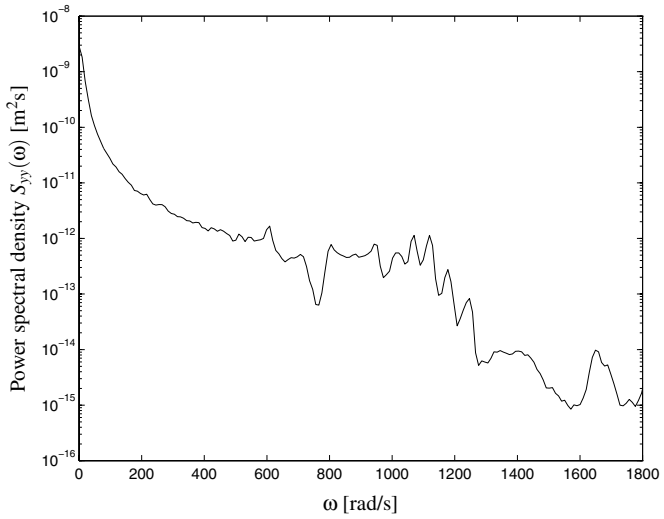

Figure 13. Power spectral density of the excitation for ω_{band} =[0.0 1226.6] rad/s.

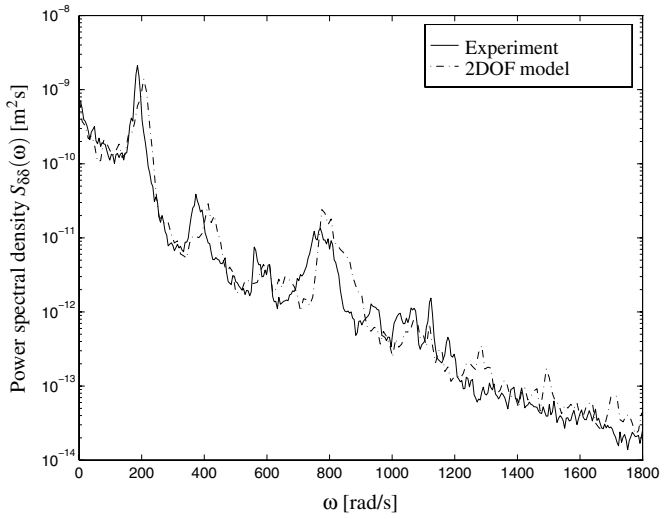

Figure 14. Comparison of the power spectral densities of δ for the experiment and the 2DOF model with ω_{band} = [0.0 1226.6] rad/s.

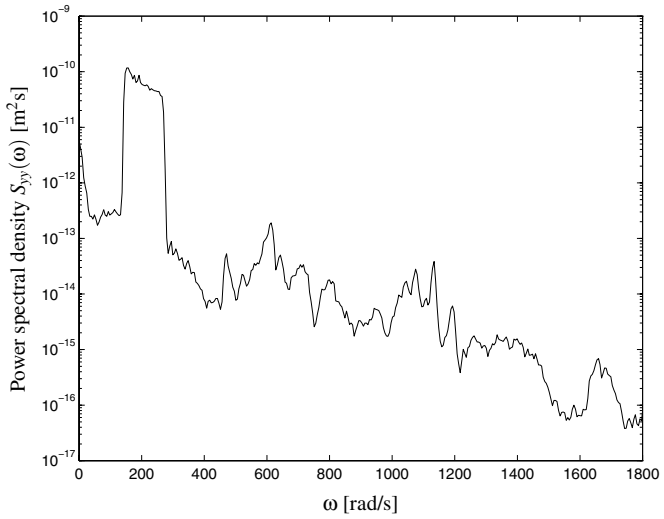

Figure 15. Power spectral density of the excitation for ω_{band} = [144.5 270.2] rad/s.

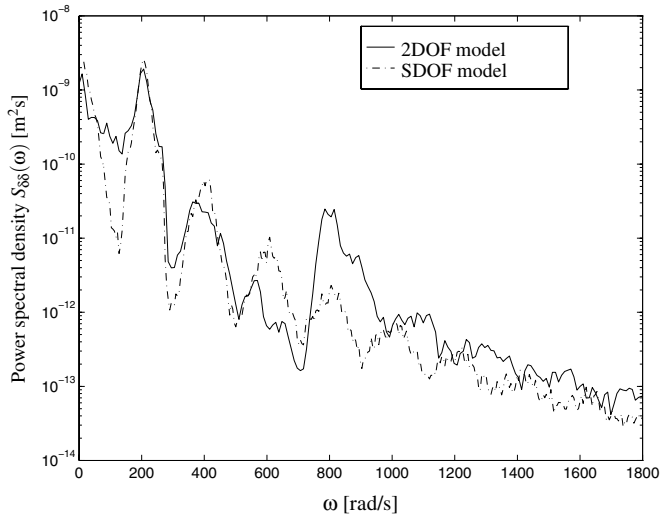

Figure 16. $S_{\delta\delta}(\omega)$ for the SDOF model and the 2DOF model for ω_{band} =[144.5 270.2] rad/s.

of low-frequency energy are clearly visible in both experimental and simulation results. However, the non-uniformity of $P_{yy}(f)$ obstructs the observation of the second characteristic. Figure 14 shows that the experimental and numerical results agree to a large extent. Clearly, the response of the 2DOF model exhibits the second harmonic resonance at $\omega = 780$ rad/s, which coincides with the experimental data. This represents an important modeling improvement in comparison to the SDOF model [5], since, obviously, the second mode is absent in the SDOF model.

In figure 16, the power spectral densities of the responses of the SDOF model an the 2DOF model for an 'experimental' [144.5 270.2] rad/s excitation (see figure 15) are compared. This figure shows that the addition of the extra degree of freedom has a significant effect on the stochastic response of the system: this effect not only expresses itself through the second (stochastic) harmonic resonance peak near 780 rad/s, but also affects the response characteristics in lower frequency ranges. Figure 17 shows that particularly this effect of the second degree of freedom makes the simulation results of the 2DOF model fit the experimental results better than the results of the SDOF model

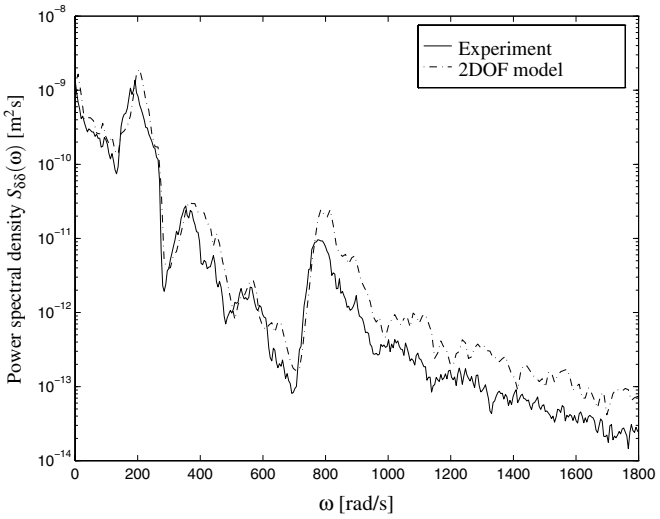

Figure 17. $S_{\delta\delta(\omega)}$ for the experiment and the 2DOF model for ω_{band} =[144.5 270.2] rad/s.

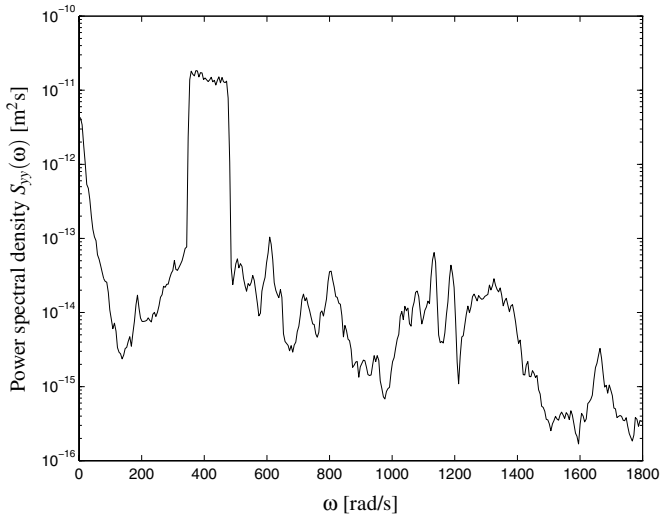

Figure 18. Power spectral density of the excitation for ω_{band} = [351.9 477.5] rad/s.

(observe, hereto, figure 16 and 17 simultaneously). The fact that the extension towards a 2DOF model also affects the response at lower frequencies corresponds to tendencies seen in the periodic response of the 2DOF model, see figure 4. However, for stochastic excitations the effect of the addition of the second degree of freedom does not seem to have such a dramatic effect on the response (at lower frequencies) as for periodic excitation. Apparently, local effects (in terms of frequency) are somehow averaged for stochastic excitations. Note, moreover, that the experimental data in figure 17 express the fact that a 'stochastic harmonic' response also appears in the experiment.

Figure 19 displays an experimental 'stochastic 1/2 subharmonic' solution, which occurs when the applied, Gaussian excitation exhibits a power spectral density as depicted in figure 18. Furthermore, figure 19 confirms once more that the 2DOF model describes all the important dynamic phenomena of the stochastic response of the experimental system very well.

Moreover, by comparing the figures 17 and 19 we can detect that the energy of both experimental stochastic solutions are of a comparable level. Note, however, that the power spectral density of the excitation in figure 18 is significantly lower than that in figure 15. So, this effect corresponds to an effect, which was also observed for the periodic and stochastic simulations, see sections 3 and 5, respectively. There, the 1/2 subharmonic solution proved to be of a higher energy level than the harmonic solution (for identical input levels).

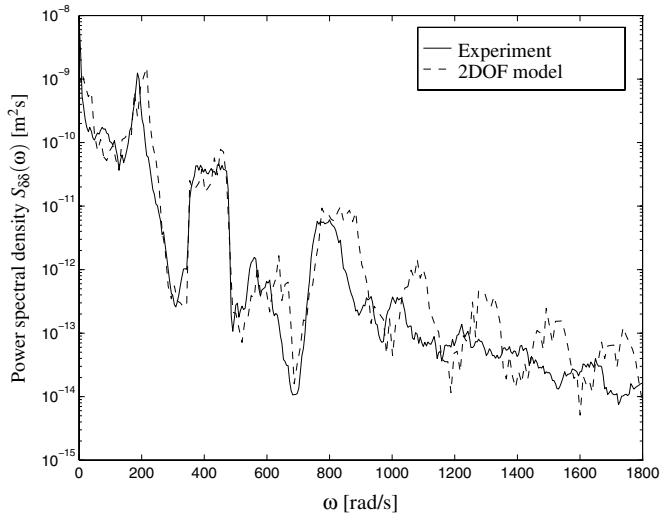

Figure 19. $S_{\delta\delta}(\omega)$ for the experiment and the 2DOF model for ω_{band} = [351.9 477.5] rad/s.

8 Conclusions

We have investigated the stochastic response phenomena of a beam-impact system under band-limited, stochastic excitation both experimentally and numerically. Clearly, the simultaneous observation of the periodic and stochastic behavior of the system proved to be very fruitful in gaining understanding with respect to the stochastic response phenomena. For a number of periodic response phenomena stochastic equivalents were presented, such as 'stochastic harmonic' and 'stochastic subharmonic' solutions. Hereto, it was important to observe the response from a frequency-domain perspective.

Moreover, it was shown that the 2DOF model can predict the stochastic behavior of the experimental system very accu-

rately. Related, hereto, it is important to note that the addition of the second mode (near 780 rad/s) does not only result in a modeling improvement near this second resonance, but also accomplishes a significant improvement for lower frequencies, when compared to the SDOF model [5]. So, even for excitation spectra up to 500 rad/s, the 2DOF model should be preferred over the SDOF model. Moreover, an extension towards a 3DOF model will most probably not yield a significantly better approximation of the experimental response characteristics, since, firstly, the 2DOF description is already very accurate for the frequency range observed in this paper. Moreover, the third mode (eigenfrequency is approximately 2300 rad/s) will become more important when one is interested in response characteristic in this 'higher' frequency range and when the excitation exhibits a significant amount of energy in this frequency range. Furthermore, an extension towards a model with more degrees of freedom will directly result in a decrease in computational efficiency, which is crucial in the numerical approximation of stochastic response characteristics. It can, therefore, be concluded that the modeling approach, in which the continuous, linear part of the beam-impact system (the elastic beam) is reduced to a two-mode description before merging it with a model for the local nonlinearity, is a valid and successful one for both periodic (see [1]) and stochastic excitations.

References

[1] Fey, R. H. B., 1992. *Steady-state behaviour of reduced dynamic systems with local nonlinearities*. Ph.D. thesis, Eindhoven University of Technology, The Netherlands.

[2] Fey, R. H. B., Van Campen, D. H., and De Kraker, A., 1996. Long term structural dynamics of mechanical systems with local nonlinearities. Trans. ASME, J. Vibration and Acoustics, **118(2)**, pp. 147–153. Also publ. in: Proc. Winter Annual Meeting ASME, Anaheim (Calif., USA), 8-13 Nov., DE-Vol. 50, AMD-Vol. 44, eds. R.A. Ibrahim and N.S. Namachchivaya, 1992, pp. 159-167.

[3] Van de Vorst, E. L. B., 1996. *Long term dynamics and stabilization of nonlinear mechanical systems*. Ph.D. thesis, Eindhoven University of Technology, The Netherlands.

[4] Van Campen, D. H., De Kraker, A., Fey, R. H. B., Van de Vorst, E. L. B., and Van der Spek, J. A. W., 1997. Long-term dynamics of nonlinear MDOF engineering systems. Chaos, Solitons and Fractals; Special Issue on Nonlinearities in Mechanical Engineering, **8(4)**, pp. 455–477.

[5] Van de Wouw, N., Van den Bosch, H. L. A., De Kraker, A., and Van Campen, D. H., 1998. Experimental and numerical analysis of nonlinear phenomena in a stochastically excited beam system with impact. Choas, Solitons & Fractals, **9(8)**, pp. 1409–1428.

[6] Meirovitch, L., 1997. *Principles and techniques of vibrations*. Prentice-Hall International, New Jersey.

[7] Van de Wouw, N., 1999. *Steady state behaviour of stochastically excited nonlinear dynamic systems*. Ph.D. thesis, Eindhoven University of Technology.

[8] Hertz, H., 1895. *Gesammelte Werke, vol. 1: Schriften Vermischten Inhalts*. J.A. Barth, Leipzig, Germany (German).

[9] Goldsmith, W., 1960. *Impact: the theory and physical behaviour of colliding solids*. E. Arnold Ltd., London.

[10] Lankarani, H. M. and Nikravesh, P. E., 1994. Continuous contact force models for impact analysis in multibody sytems. Nonlinear Dynamics, **5**, pp. 193 – 207.

[11] Van de Vorst, E., Heertjes, M., Van Campen, D., De Kraker, A., and Fey, R., 1998. Experimental and numerical analysis of the steady-state behaviour of a beam system with impact. Journal of Sound and Vibration, **212(2)**, pp. 321–336.

[12] Shinozuka, M., 1972. Monte Carlo Solution of structural Dynamics. Computers & Structures, **2**, pp. 855–874.

[13] Yang, J.-N., 1972. Simulation of Random Envelope Processes. Journal of Sound and Vibration, **21(1)**, pp. 73–85.

[14] Hénon, M., 1982. On the numerical computation of Poincaré maps. Journal of Applied Mechanics, **47**, pp. 931 – 939.

[15] Shaw, S. W. and Holmes, P. J., 1983. A periodically forced piecewise linear oscillator. Journal of Sound and Vibration, **90(1)**, pp. 129–155.

[16] Roberts, J. B. and Spanos, P. D., 1990. *Random vibration and statistical linearization*. John Wiley and Sons, New York.

[17] DIFA, 1992. *FA100 User Manual*. DIFA Measuring Systems, Breda, The Netherlands.